

# Human-in-the-Loop Feature Selection Using Interpretable Kolmogorov-Arnold Network-based Double Deep Q-Network

Md Abrar Jahin, M. F. Mridha, *Senior Member, IEEE*, and Nilanjan Dey, *Senior Member, IEEE*

**Abstract**—Feature selection is critical for improving the performance and interpretability of machine learning models, particularly in high-dimensional spaces where complex feature interactions can reduce accuracy and increase computational demands. Existing approaches often rely on static feature subsets or manual intervention, limiting adaptability and scalability. However, dynamic, per-instance feature selection methods and model-specific interpretability in reinforcement learning remain underexplored. This study proposes a human-in-the-loop (HITL) feature selection framework integrated into a Double Deep Q-Network (DDQN) using a Kolmogorov-Arnold Network (KAN). Our novel approach leverages simulated human feedback and stochastic distribution-based sampling, specifically Beta, to iteratively refine feature subsets per data instance, improving flexibility in feature selection. The KAN-DDQN achieved notable test accuracies of 93% on MNIST and 83% on FashionMNIST, outperforming conventional MLP-DDQN models by up to 9%. The KAN-based model provided high interpretability via symbolic representation while using 4 times fewer neurons in the hidden layer than MLPs did. Comparatively, the models without feature selection achieved test accuracies of only 58% on MNIST and 64% on FashionMNIST, highlighting significant gains with our framework. Pruning and visualization further enhanced model transparency by elucidating decision pathways. These findings present a scalable, interpretable solution for feature selection that is suitable for applications requiring real-time, adaptive decision-making with minimal human oversight.

**Index Terms**—Human-in-the-Loop, Feature Selection, Kolmogorov Arnold Network, Reinforcement Learning, Double Deep Q-Network.

## I. INTRODUCTION

**F**EATURE selection is essential for building efficient, accurate, and robust machine learning models [1, 2]. While models ideally should automatically identify the most predictive features, a high-dimensional input space can significantly hinder performance, often requiring large volumes of data to learn from the complex relationships between features effectively. This phenomenon, known as the “curse of dimensionality,” increases computation time and resource use. Consequently, selecting a smaller subset of relevant features improves performance and makes the model more cost-effective.

M. A. Jahin is with Okinawa Institute of Science and Technology Graduate University, Okinawa 904-0412, Japan (e-mail: abrar.jahin.2652@gmail.com).

M. F. Mridha is with the Department of Computer Science, American International University-Bangladesh, Dhaka 1229, Bangladesh (e-mail: firoz.mridha@aiub.edu).

N. Dey is with the Department of Computer Science & Engineering, Techno International New Town, New Town, Kolkata, 700156, India (e-mail: nilanjan.dey@tint.edu.in).

One common solution is to incorporate expert knowledge to determine the most useful features; however, this process is costly, time-consuming, and highly manual. Additionally, experts with deep domain knowledge are often not involved in the actual design and development of the model. Automatic feature selection methods offer an alternative, ranking features by their relevance or importance; however, both manual and automatic approaches typically yield a single subset of features for the entire dataset, which may not capture variability across individual observations. When training data are sparse relative to the feature space, the use of a single subset can limit the model’s ability to generalize effectively across all instances [3].

To address the challenge of per-example feature selection, we propose a reinforcement learning (RL) framework that leverages simulated feedback to replicate human feature selection. Our approach employs a Double Deep Q-Network (DDQN) setup with a Kolmogorov-Arnold Network (KAN) as both the Q and target networks. This model-specific interpretable KAN-based RL structure aims to refine feature selection on a per-example basis iteratively. In this setup, simulated feedback, rather than direct human input, is a proxy for expert annotation. The feedback signal highlights the most relevant features for each data example, creating a pathway for the model to prioritize these features during training. Unlike prior methods, our model explores distributions beyond Bernoulli and organizes convolutional and pooling layers to ensure feature maps match the input and simulated feedback shapes. RL then optimizes a policy to select a unique subset of features per observation. By minimizing the classifier’s prediction loss and the discrepancy between simulated feedback and the model-selected features, this policy yields feature subsets that improve the interpretability and performance of the final predictions. Since predictions are based only on the selected feature subsets, this method offers interpretable, case-specific insights into the model’s output. Using simulated feedback further enables the model to reflect causal structures likely to be relevant in practical applications. We validate our methodology through rigorous experimentation on benchmark datasets, showing the efficiency of our approach in improving model accuracy while maintaining computational feasibility. We aim to establish best practices for integrating human feedback into the feature selection process by investigating the influence of various hyperparameters, stochastic distributions, and the absence of feature selection.

The key components of our contribution include the follow-

ing:

- 1) We introduce a novel approach incorporating simulated feedback via Gaussian heatmaps and stochastic, distribution-based sampling to refine feature subsets on a per-example basis, thereby enhancing model interpretability and performance.
- 2) By incorporating KAN into the DDQN architecture for both the Q-network and target network, we achieve significantly better performance than traditional MLP-based DDQN across all test cases. This approach uses a hidden layer with four times fewer neurons than MLP while offering model-specific interpretability.
- 3) Our research presents a simulated feedback mechanism that generates feature relevance feedback without human annotators, facilitating a scalable training process that reflects the causal relationships typically identified by human experts.

The following sections provide an overview of our work: Section II reviews the relevant background; Section III outlines the complete methodology of our proposed framework; Section IV details the experimental design; Section V discusses the results and their interpretations; and finally, Section VI concludes the research while outlining potential future directions.

## II. BACKGROUND

### A. Human-in-the-Loop Feature Selection Using RL

Feature selection is critical in developing machine learning models but is often executed through data-driven methods that overlook insights from human designers [2, 4]. We introduce a HITL [5] framework that integrates simulated feedback to identify the most relevant variables for specific tasks, which can be modeled using DDQN-based [6] RL to facilitate per-example feature selection [7], enabling the model to minimize its loss function while emphasizing significant variables from a simulated human perspective. A major gap in RL is the limited model-specific interpretability, as most models operate as black-box systems, making it challenging to understand their decision-making processes [8]. Our KAN agent enhances the interpretability of DDQN-based RL by providing symbolic representations of learned policies. Our methodology employs variable elimination techniques, focusing on selecting subsets of features rather than using embedded methods. This approach optimizes feature selection and learning processes concurrently via gradient descent and distinguishes itself by selecting different subsets for each observation. This enhances interpretability, as the chosen variables represent the “causes” driving the model’s predictions. While previous work [1, 5] has explored per-example feature selection via traditional filter methods based on mutual information, our framework goes beyond incorporating simulated human feedback for a more dynamic approach. Traditional feature selection techniques include filter methods, which select top-ranked features based on criteria like mutual information; wrapper methods, which evaluate subsets of features by retraining models for each subset; and embedded methods, which attempt to select features during the model training process. Unlike these approaches,

which can be sequential and computationally costly, our model generates candidate subsets in a single step, guided by simulated feedback, thereby avoiding arbitrary stopping criteria and allowing for real-time, per-example selection in complex datasets. Our work draws inspiration from the probabilistic knowledge elicitation [9, 10] focused on querying users for global feature relevance. However, our model goes beyond the focus on Bernoulli distributions [3] by exploring various distributions, including beta, Gaussian, and Gumbel-Softmax, enhancing the flexibility and effectiveness of feature selection. This breadth allows us to capture a wider range of relationships within the data compared with previous approaches.

### B. Kolmogorov-Arnold Networks (KANs)

KANs [11] utilize the Kolmogorov-Arnold representation theorem, which states that any multivariate continuous function  $f : [0, 1]^n \rightarrow \mathbb{R}$  can be expressed as a finite composition of univariate functions and additions. Mathematically, this is formulated as follows:

$$f(x) = \sum_{q=1}^{2^{n+1}} \Phi_q \left( \sum_{p=1}^n \phi_{q,p}(x_p) \right) \quad (1)$$

where  $\phi_{q,p} : [0, 1] \rightarrow \mathbb{R}$  and  $\Phi_q : \mathbb{R} \rightarrow \mathbb{R}$  are continuous functions. In KANs, the traditional weight parameters are substituted with learnable one-dimensional B-spline functions  $\phi$ . The output of a KAN layer with  $n_{in}$  inputs and  $n_{out}$  outputs is given by:

$$x_{l+1,j} = \sum_{i=1}^{n_l} \phi_{l,j,i}(x_{l,i}) \quad (2)$$

where  $\phi_{l,j,i}$  connects the  $i$ -th neuron in layer  $l$  to the  $j$ -th neuron in layer  $l+1$ . The backpropagation algorithm computes gradients with respect to the spline coefficients  $c_i$  to minimize the loss  $L$  via gradient descent:

$$\frac{\partial L}{\partial c_i} = \sum_{j=1}^{n_{out}} \frac{\partial L}{\partial x_{l+1,j}} \frac{\partial x_{l+1,j}}{\partial c_i} \quad (3)$$

where  $\frac{\partial x_{l+1,j}}{\partial c_i}$  reflects the derivative of the spline function concerning its coefficients. KANs define spline functions  $\phi$  over a discretized grid, which specifies where the functions are evaluated, thus influencing the approximation resolution. The order parameter indicates the degree of the B-splines: an order of 1 denotes linear splines, while higher orders yield more complex shapes. The grid and order parameters determine KANs’ capacity to model intricate functional relationships; finer grids with higher-order splines allow for precise approximations but require more computational resources.

The differences between KAN and MLP are that KANs implement learnable activation functions along edges, contrasting with MLPs, which implement fixed activation functions at nodes. KANs represent weights as splines, improving their ability to approximate complex functions with fewer parameters. KANs and MLPs can be extended to multiple layers, supporting deep architectures.

---

**Algorithm 1:** FSNet Model Initialization and Forward Pass
 

---

**Input:** Input shape  $input\_shape$ , Number of filters  $num\_filters$ , Number of convolutional layers  $num\_conv\_layers$ , Hidden layer dimension  $hidden\_dim$ , Distribution  $distribution$ , Temperature parameter  $\tau$

**Result:** Processed feature map, feedback cost, feature probabilities

```

1 Function FSNet( $input\_shape, num\_filters,$ 
   $num\_conv\_layers, hidden\_dim, distribution, \tau$ ):
2   Initialize convolutional layer parameters:
      $channels \leftarrow []$ ; for  $i \leftarrow 1$  to  $num\_conv\_layers$ 
     do
3      $num\_filters \leftarrow num\_filters \times 2$ ;
4     Append  $num\_filters$  to  $channels$ ;
5   Build feature extractor with  $num\_conv\_layers$ 
     Conv2D, ReLU, and MaxPool layers;
6   Initialize fully connected layer  $fc1$  with input size
      $n\_features$  and hidden size  $hidden\_dim$ ;
7   Initialize output layer  $fc2$  with input size
      $hidden\_dim$  and output size  $n\_features$ ;
8   Initialize activation functions:  $relu$ ,  $sigmoid$ , and
      $softmax$ ;

9 Function forward( $x, feedback, epoch$ ):
10  Reshape  $x$  to match  $input\_shape$ ;
11   $features \leftarrow$  Pass  $x$  through feature extractor;
12   $x \leftarrow relu(fc1(features))$ ;
13  Compute  $logits \leftarrow relu(fc2(x))$ ;
14  Compute feature selection probabilities
      $probs \leftarrow sigmoid(logits)$ ;
15  if  $feedback$  is None then
16  |  $feedback \leftarrow probs$ ;
17  Sample  $sample\_probs$  from  $distribution$  using
      $logits$  as parameters;
18  Adjust temperature parameter if Gumbel-Softmax
     is used:  $tau \leftarrow \tau \times \tau\_decay^{epoch}$ ;
19  Calculate feedback cost  $feedback\_cost \leftarrow$ 
      $MSE\_Loss(probs, feedback)$ ;
20   $selected\_feature \leftarrow features \times sample\_probs$ ;
21  return  $selected\_feature, feedback\_cost, probs$ ;

```

---

### III. METHODOLOGY

#### A. Human-in-the-Loop Feature Selection Process

The feature selection network (FSNet) (see Algorithm 1) is designed to determine the relevance of each input feature for a given task. The architecture combines convolutional layers for feature extraction with various probabilistic distributions to model and sample feature importance. Here, we detail each model component, focusing on architectural elements, distribution-based sampling, and feedback alignment.

1) *Convolutional Feature Extraction Layers:* The first stage of FSNet involves convolutional layers that transform the input tensor  $x$  into feature representations that capture important

patterns across spatial dimensions. Suppose  $x \in \mathbb{R}^{d \times h \times w}$  represents an input with  $d$  channels, height  $h$ , and width  $w$ . The convolutional feature extractor uses  $L$  layers of convolution, ReLU activation, and max-pooling to refine the spatial features of the input progressively. For layer  $i$ , with filter count  $f_i$ , the transformation can be expressed as:

$$F^{(i)} = \text{MaxPool2d}(\text{ReLU}(\text{Conv2d}(F^{(i-1)}))) \quad (4)$$

where  $F^{(i)} \in \mathbb{R}^{f_i \times \frac{h}{2^i} \times \frac{w}{2^i}}$  and  $F^{(0)} = x$ . Each convolutional layer uses a  $3 \times 3$  kernel and padding of 1 to maintain spatial dimensions, while max-pooling layers with kernel size 2 reduce the height and width by half at each step.

2) *Fully Connected Layers for Feature Probability Mapping:* After convolutional layers, the resulting feature map is flattened and processed by fully connected layers to output feature relevance scores (logits). Let  $F \in \mathbb{R}^n$  represent the flattened feature vector, where  $n$  is the number of features output by the convolutional layers. This vector is then passed through a sequence of fully connected (FC) layers, ReLU activation, and dropout:

$$h = \text{ReLU}(W_{fc1} \cdot F + b_{fc1}) \quad (5)$$

where  $h \in \mathbb{R}^{128}$  (if 128 hidden units are used),  $W_{fc1} \in \mathbb{R}^{128 \times n}$  is the weight matrix, and  $b_{fc1} \in \mathbb{R}^{128}$  is the bias vector. The ReLU introduces non-linearity, while dropout (with a rate of 0.25) mitigates overfitting. Finally, the output layer applies a sigmoid function to yield probability values for each feature:

$$\hat{q} = \sigma(W_{fc2} \cdot h + b_{fc2}) \quad (6)$$

where  $\hat{q} = (\hat{q}_1, \hat{q}_2, \dots, \hat{q}_d)$  represents the probability score for each feature. The sigmoid activation ensures that  $\hat{q}_j \in [0, 1]$  for all  $j$ , making  $\hat{q}$  interpretable as a relevance score or probability vector and  $\sigma(z) = \frac{1}{1+e^{-z}}$  is the sigmoid function.

3) *Distribution-Based Sampling for Probabilistic Feature Selection:* In our framework, feature selection is modeled as a probabilistic policy  $\pi(a | \hat{q})$ , where each feature selection mask  $a \in \{0, 1\}^d$  is sampled based on a probability vector  $\hat{q} = (\hat{q}_1, \hat{q}_2, \dots, \hat{q}_d)$ . This vector  $\hat{q}$ , derived from the network output, represents the relevance probability of each feature. For a given action  $a$  (or feature mask), the policy is defined as:

$$\pi(a | \hat{q}) = \prod_{j=1}^d P(a_j | \hat{q}_j) \quad (7)$$

where  $P(a_j | \hat{q}_j)$  is the probability of selecting (or discarding) each feature  $j$  based on a chosen distribution. Using this probabilistic policy allows flexibility in feature selection while controlling each selection probability by the network's learned relevance score  $\hat{q}_j$ . The feature mask  $a$  is generated according to various probabilistic distributions described below.

**Bernoulli Distribution Sampling:** In Bernoulli distribution sampling, each feature's selection is modeled as an independent binary random variable, where each feature  $j$  is selected with a probability  $\hat{q}_j$  derived from the network's sigmoid output.

$$a_j \sim \text{Bernoulli}(\hat{q}_j) \quad (8)$$

where  $\hat{q}_j \in [0, 1]$  represents the probability of selecting feature  $j$ . If  $a_j = 1$ , feature  $j$  is retained; if  $a_j = 0$ , feature  $j$  is discarded.

**Gumbel-Softmax Sampling:** Gumbel-Softmax distribution provides a differentiable approximation to categorical sampling. For each feature  $j$ , the mask  $a_j$  is computed as:

$$a_j = \frac{\exp((\log \hat{q}_j + g_j)/\tau)}{\sum_{k=1}^d \exp((\log \hat{q}_k + g_k)/\tau)} \quad (9)$$

where  $g_j \sim \text{Gumbel}(0, 1)$  and the temperature  $\tau$  decays over time.

**Gaussian Distribution Sampling:** Each feature selection probability  $\hat{q}_j$  is used as the mean  $\mu_j$  of a Gaussian distribution with fixed standard deviation  $\sigma = 1$ :

$$a_j \sim \mathcal{N}(\mu_j = \hat{q}_j, \sigma = 1) \quad (10)$$

This sampling scheme maintains smooth variations around  $\hat{q}_j$ .

**Beta Distribution Sampling:** Beta distribution, bounded between 0 and 1, provides flexibility in modeling the probability  $\hat{q}_j$  with shape parameters  $\alpha_j$  and  $\beta_j$ :

$$a_j \sim \text{Beta}(\alpha_j, \beta_j), \quad \alpha_j = \beta_j = \text{softplus}(\hat{q}_j) + 1 \quad (11)$$

Beta distribution allows for high flexibility in the shape of the probability distribution, which can vary significantly depending on  $\hat{q}_j$ . For example, if  $\hat{q}_j$  is close to 1, the distribution skews towards retaining the feature; if  $\hat{q}_j$  is close to 0, it skews towards discarding it.

**Dirichlet Distribution Sampling:** For interdependent feature probabilities, we generalize to the Dirichlet distribution, where each  $\hat{q}_j$  represents a concentration parameter:

$$\mathbf{a} \sim \text{Dirichlet}(\alpha), \quad \alpha_j = \text{softplus}(\hat{q}_j) + 1 \quad (12)$$

where  $\alpha = (\alpha_1, \alpha_2, \dots, \alpha_d)$  is the vector of concentration parameters.

**Multinomial Distribution Sampling:** In multinomial sampling, we interpret  $\hat{q} = (\hat{q}_1, \hat{q}_2, \dots, \hat{q}_d)$  as logits:

$$\mathbf{a} \sim \text{Multinomial}(n = 1, p = \sigma(\hat{q})) \quad (13)$$

where  $p$  is the probability distribution over the features given by applying softmax to  $q$  and  $n = 1$  indicates that we are drawing a single sample. This approach allows for categorical selection from among the features based on the probability distribution defined by  $q$ .

**Laplace Distribution Sampling:** In Laplace sampling, each  $\hat{q}_j$  serves as the mean  $\mu_j$  for the Laplace distribution:

$$a_j \sim \text{Laplace}(\mu_j = \hat{q}_j, \text{scale} = 1) \quad (14)$$

**Cauchy Distribution Sampling:** For Cauchy distribution sampling, each  $\hat{q}_j$  is the location parameter:

$$a_j \sim \text{Cauchy}(\text{location} = \hat{q}_j, \text{scale} = 1) \quad (15)$$

The Cauchy distribution has no well-defined mean or variance, making it highly sensitive to extreme values. This can result in selective or random feature activation depending on the value of  $\hat{q}_j$ , which introduces higher variability in feature selection.

**Uniform Distribution Sampling:** Uniform sampling considers each  $a_j$  equally probable within  $[0, 1]$ :

$$a_j \sim \text{Uniform}(0, 1) \quad (16)$$

The sampled feature mask  $\mathbf{a}$  is then applied to the feature vector  $\mathbf{f}$  as:

$$\mathbf{f}_{\text{selected}} = \mathbf{f} \odot \mathbf{a} \quad (17)$$

where  $\odot$  denotes element-wise multiplication, yielding a filtered feature vector  $\mathbf{f}_{\text{selected}}$  that selectively retains features based on their relevance.

4) *Feedback Alignment with MSE Loss:* FSNet uses mean squared error (MSE) to align the model’s feature relevance scores with human-provided feedback. Let  $f \in \mathbb{R}^d$  represent a feedback vector where each  $f_j \in [0, 1]$  indicates human-assessed importance for feature  $j$ . The feedback cost function  $C_f$  is defined as:

$$\mathcal{L}_{\text{feedback}} = C_f(x; \hat{q}, f) = \mathbb{E} [\|f - \hat{q}\|^2] = \frac{1}{d} \sum_{j=1}^d (f_j - \hat{q}_j)^2 \quad (18)$$

This loss function penalizes discrepancies between the model’s probability vector  $\hat{q}$  and the feedback  $f$ . Minimizing  $C_f$  encourages FSNet to produce relevance scores that align with human intuition, resulting in a more interpretable feature selection.

## B. Double Deep Q-Network Architecture

The DDQN architecture in our approach extends the traditional Q-learning framework by employing two neural networks: the primary Q-network, denoted as  $Q_\theta$ , and a target network, denoted as  $Q_{\theta'}$ . The primary Q-network learns the action-value function  $Q(s, a; \theta)$ , estimating the expected cumulative reward for selecting action  $a$  in a given state  $s$ . To stabilize training and mitigate the overestimation bias commonly observed in standard Q-learning, we use the target network  $Q_{\theta'}$ , updated less frequently than the primary network.

During training, the parameters of  $Q_\theta$  are updated via gradient descent, while the parameters of  $Q_{\theta'}$  are periodically synchronized with  $Q_\theta$  to avoid target instability. To update  $Q(s, a; \theta)$  toward the target (Equation 20), we leverage a replay buffer  $\mathcal{B}$ , which stores experience tuples  $(s, a, r, s')$ . Sampling mini-batches from  $\mathcal{B}$  helps reduce correlations between consecutive experiences, improving stability and allowing for independent updates to Q-values.

## C. KAN

In our approach, the KAN-based architecture is structured with widths of  $[64, 8, 10]$  for the input, hidden, and output layers. Both the Q-network and target network use this compact configuration to capture complex feature interactions efficiently. Each KAN layer combines a spline function and a residual basis function, formulated as:

$$\phi(x) = w_b b(x) + w_s \text{spline}(x) \quad (19)$$

**Algorithm 2:** Training Procedure for DDQN Model

---

**Input:** Configuration *config*, containing training hyperparameters

**Output:** Trained Q-network, performance metrics

- 1 Initialize environment  $\mathcal{E}$ , replay buffer  $\mathcal{B}$  with capacity *buffer\_size*;
- 2 Define  $Q_\theta$ , the Q-network, and  $Q_{\theta'}$ , the target network;
- 3 Initialize optimizer with *learning\_rate* and *weight\_decay*;
- 4 Define the learning rate scheduler with decay factor  $\gamma$ ;
- 5 **for** each epoch  $t = 1, 2, \dots, n\_epochs$  **do**
- 6   Initialize training metrics: running loss, correct predictions, feedback cost;
- 7   **for** each batch  $b$  in environment  $\mathcal{E}$  **do**
- 8     Obtain current state  $s$ , label  $y$ , and feedback from environment;
- 9     **if** *feature\_selection* is *True* **then**
- 10       Apply feature selection using agent, compute feedback cost and probabilities;
- 11       Store feedback cost and probabilities;
- 12       Update  $s \leftarrow$  processed state;
- 13     **else**
- 14       Use raw state;
- 15     Choose action  $a$  using  $\epsilon$ -greedy on  $Q_\theta$  or random action if warm-up;
- 16     Compute reward based on  $a$  and  $y$ ;
- 17     Obtain next state  $s'$ , apply feature selection if enabled;
- 18     Store  $(s, a, s', r)$  in  $\mathcal{B}$ ;
- 19     **if** *buffer*  $\mathcal{B}$  is ready (*size* > *batch\_size*) **then**
- 20       Sample a batch from  $\mathcal{B}$ ;
- 21       Compute Q-learning target  $y = r + \gamma \max_{a'} Q_{\theta'}(s', a')$ ;
- 22       Compute current estimate  $Q_\theta(s, a)$ ;
- 23       Compute combined loss using  $\mathcal{L}_{\text{SmoothL1}}$  with regularization;
- 24       **if** *feature\_selection* is *True* **then**
- 25         Add feedback cost to loss;
- 26       Backpropagate loss and update  $Q_\theta$ ;
- 27     **if**  $t \bmod 25 = 0$  and *method* is "KAN" and  $t < \frac{n\_epochs}{2}$  **then**
- 28       Update grid of  $Q_\theta$  and  $Q_{\theta'}$  with samples from  $\mathcal{B}$ ;
- 29     **if**  $t \bmod target\_update = 0$  **then**
- 30       Update target  $Q_{\theta'} \leftarrow Q_\theta$ ;
- 31     Adjust learning rate with scheduler;
- 32 Return  $Q_\theta$  and collected metrics (accuracy, loss, feedback cost history);

---

where  $b(x) = \text{silu}(x)$  serves as a non-linear basis function, while  $\text{spline}(x) = \sum_i c_i B_i(x)$  utilizes trainable B-splines for flexible approximation. With spline order  $k = 3$  over a specified grid, this layered structure dynamically adjusts to

feature relevance throughout training. For optimization,  $w_b$  and  $w_s$  are initialized carefully:  $w_b$  uses Xavier initialization, ensuring balanced layer activation scales, while  $w_s$  is set to 1, with the initial spline function close to zero. The model's spline grids adapt to changing input activations, extending KAN's effective region for learning. By leveraging these optimizations and not training biases or spline parameters directly, the KAN achieves significant performance gains with reduced neurons in the hidden layer—showing a parameter-efficient architecture that improves interpretability.

**D. MLP**

The MLP-based architecture provides a more traditional setup for the DDQN framework, using a straightforward, fully connected design for both the Q-network and the target network. This configuration includes 2 linear layers: a 64-neuron initial layer to map the input features to a hidden space defined by a 32-neuron network width, followed by a ReLU activation, and a 10-neuron final linear layer to produce Q-values. The MLP requires a larger hidden layer with 32 neurons to approximate the complex mappings found in datasets, making it parameter-heavy relative to the KAN-based DDQN.

**E. Training Procedure: KAN-based and MLP-based DDQN**

The training procedure for the DDQN is illustrated in Algorithm 2, which outlines the main steps taken during each epoch. The algorithm initializes the environment and Q-networks and iteratively processes batches of experiences from a replay buffer  $\mathcal{B}$ . Each experience consists of the current state  $s$ , action  $a$ , reward  $r$ , and the next state  $s'$ .

We employ two training algorithms to optimize our Q-network, each tailored to different model architectures: (1) a KAN-based training procedure that utilizes regularization for interpretability and stability and (2) a standard MLP-based training procedure. Each training procedure integrates feedback cost when feature selection is enabled, promoting a minimalistic and interpretable feature set.

1) *Temporal-Difference Target Computation:* Both KAN and MLP-based approaches utilize the temporal-difference (TD) target to stabilize Q-learning updates and reduce the discrepancy between estimated Q-values and TD targets. For a given experience tuple  $(s, a, s', r, d)$ , where  $s$  and  $s'$  represent the current and next states,  $a$  is the action taken,  $r$  is the reward, and  $d$  indicates the termination flag, the TD target is computed as:

$$\text{TD\_target} = r + \gamma Q_{\theta'} \left( s', \arg \max_a Q_\theta(s', a) \right) \quad (20)$$

where  $\gamma \in [0, 1]$  is the discount factor for future rewards. Here,  $Q_\theta(s', a)$  determines the action  $a$  that maximizes the Q-value for the next state  $s'$ , and  $Q_{\theta'}$  provides the stable estimate for this chosen action. The target network  $Q_{\theta'}$ , updated less frequently, offers a stable estimation for TD updates.

2) *KAN-based Training with Regularization*: In the KAN-based training procedure, we employ *SmoothL1* loss, which has proven effective in mitigating the influence of large outliers in Q-value errors. The primary loss term  $\mathcal{L}_{TD}$  is given by:

$$\mathcal{L}_{TD} = L_\delta(Q_\theta(s, a) - TD\_target) \quad (21)$$

where  $L_\delta$  represents the *SmoothL1* loss:

$$L_\delta(x) = \begin{cases} 0.5x^2 & \text{if } |x| < 1 \\ |x| - 0.5 & \text{otherwise} \end{cases} \quad (22)$$

*L1 and Entropy-Based Regularization*: In KANs, the L1 norm is applied to encourage sparsity in the activation functions, which replaces traditional linear weights used in MLPs. The L1 norm of an activation function  $\phi$  is defined as the average magnitude of its outputs over  $N_p$  inputs:

$$\|\phi\|_1 \equiv \frac{1}{N_p} \sum_{s=1}^{N_p} \phi(x^{(s)}) \quad (23)$$

For a KAN layer  $\Phi$  with  $n_{in}$  inputs and  $n_{out}$  outputs, we define the L1 norm of  $\Phi$  as the sum of the L1 norms of all activation functions:

$$\|\Phi\|_1 \equiv \sum_{i=1}^{n_{in}} \sum_{j=1}^{n_{out}} \|\phi_{i,j}\|_1. \quad (24)$$

In addition, an entropy term is introduced to reduce overconfidence in the predictions. The entropy  $S(\Phi)$  for the KAN layer is given by:

$$S(\Phi) \equiv - \sum_{i=1}^{n_{in}} \sum_{j=1}^{n_{out}} \frac{|\phi_{i,j}|_1}{|\Phi|_1} \log \left( \frac{|\phi_{i,j}|_1}{|\Phi|_1} \right) \quad (25)$$

The combined regularization term is defined as:

$$\mathcal{R}_{L1+Entropy} = \sum_{i=1}^n (\lambda_{L1} \|\text{acts\_scale}_i\|_1 - \lambda_{entropy} H(\text{acts\_scale}_i)) \quad (26)$$

where  $H(\text{acts\_scale}_i) = - \sum p \log(p)$  denotes entropy with  $p$  being the normalized activation values, and  $\lambda_{L1}$  and  $\lambda_{entropy}$  are hyperparameters.

*Spline-Based Regularization*: This term regularizes the spline coefficients of the KAN activation functions, encouraging smooth transitions and sparsity in the feature space. Given the spline coefficient vector  $\text{coef}_i$  of each activation function, we compute the following:

$$\mathcal{R}_{Spline} = \sum_{i=1}^n (\lambda_{coef} \|\text{coef}_i\|_1 + \lambda_{coefdif} \|\text{diff}(\text{coef}_i)\|_1) \quad (27)$$

where  $\text{diff}(\text{coef}_i)$  calculates the adjacent differences within  $\text{coef}_i$ , enforcing smoothness in the function and preventing rapid oscillations in the learned coefficients. The combined regularization term  $\mathcal{R}$  is added to the loss as follows:

$$\mathcal{L}_{KAN} = \mathcal{L}_{TD} + \lambda \mathcal{R} = L_\delta(Q_\theta(s, a), TD\_target) + \lambda (\mathcal{R}_{L1+Entropy} + \mathcal{R}_{Spline}) \quad (28)$$

3) *Feedback Cost Integration for Feature Selection*: To minimize unnecessary feature dependencies, we incorporate a feedback cost  $\mathcal{L}_{feedback}$  (Equation 18) into the total loss with an  $\alpha = 0.5$  when feature selection is enabled. This cost penalizes selected features based on their contribution to the model, defined as follows:

$$\mathcal{L}_{KAN, total} = \mathcal{L}_{KAN} + \alpha \times \mathcal{L}_{feedback} \quad (29)$$

4) *MLP-based Training*: For the MLP-based training, we use the same TD target computation and *SmoothL1* loss but omit the KAN-specific regularization terms. Like KAN-based training, feature selection introduces an additional feedback cost term to this loss:  $\mathcal{L}_{MLP, total} = L_\delta(Q_\theta(s, a), TD\_target) + \alpha \times \mathcal{L}_{feedback}$ .

5) *Optimization and Gradient Clipping*: To ensure stable training and mitigate the risk of exploding gradients, we apply in-place gradient clipping with a threshold of 100 to both KAN and MLP-based training. This process limits the magnitude of gradients, preventing extreme updates that could destabilize the learning process:  $\text{clip}(\frac{\partial \mathcal{L}}{\partial \theta}, 100)$ . The gradients are then backpropagated, and the optimizer updates the network weights to minimize  $\mathcal{L}_{KAN, total}$  in KAN and  $\mathcal{L}_{MLP, total}$  in MLP model.

## F. Integration of HITL Feedback in DDQN

Integrating HITL feedback into the DDQN architecture enables the model to iteratively improve its feature selection by incorporating human expertise. This process adjusts the feature selection probabilities  $\hat{q}_j$  based on human feedback, leading to an improved and rationale-aware selection policy.

### 1) Feature Selection Adjustment Using HITL Feedback:

For each feature  $j$ , HITL feedback provides a target value  $f_j$ , representing the importance of that feature according to human assessment. The DDQN uses this feedback to adjust the selected feature probabilities by minimizing the feedback cost  $\mathcal{L}_{feedback}$ , thereby aligning the DDQN's policy with human expertise.

### 2) Action-Selection Policy with HITL Feedback:

The DDQN framework selects actions via an  $\epsilon$ -greedy policy, which balances exploration and exploitation. At the start of training,  $\epsilon$  is set to a high value, allowing the agent to explore actions and discover potentially valuable states randomly. Over time,  $\epsilon$  gradually decays, encouraging the agent to exploit its learned policy by selecting actions that maximize the estimated Q-value from the primary  $Q_\theta$  network:

$$a = \begin{cases} \text{random action} & \text{with probability } \epsilon \\ \arg \max_{a'} Q(s, a'; \theta) & \text{with probability } 1 - \epsilon \end{cases} \quad (30)$$

This approach improves learning by promoting diverse experiences early on while progressively focusing on reliable, high-reward actions as training progresses. When HITL feedback is introduced, the DDQN updates its policy to emphasize features positively reinforced by feedback, using this guidance to improve feature selection iteratively and refine the policy across epochs. Therefore, this  $\epsilon$ -greedy mechanism prevents premature convergence to suboptimal policies, supporting more robust training for effective feature selection.

3) *Iterative Learning Process*: The training loop for DDQN, with HITL feedback, ensures that the Q-network  $Q_\theta$  converges to an optimal feature selection policy. At each epoch, the Q-network’s weights are updated based on both the Q-learning target and the feedback cost. This iterative process continues as:

$$\theta \leftarrow \theta - \eta \nabla_\theta \mathcal{L}_{\text{total}} \quad (31)$$

where  $\eta$  is the learning rate and  $\alpha$  is a hyperparameter balancing the feedback cost and Q-network loss. By adjusting  $\alpha$  over time, the DDQN increasingly aligns its feature selection with human insights, resulting in a more interpretable and effective feature set.

#### IV. EXPERIMENTAL DESIGN

##### A. Dataset Preparation

We used a benchmark environment to standardize data preparation, feedback simulation, and visualizations across two datasets—MNIST and FashionMNIST. Each dataset was resized to a standardized input dimension of  $8 \times 8$  pixels, with normalization applied based on empirically computed means and standard deviations specific to each dataset to aid in training convergence. For MNIST, we used a mean ( $\mu$ ) of 0.1307 and a standard deviation ( $\sigma_{SD}$ ) of 0.3081, while for FashionMNIST, the  $\mu$  and  $\sigma_{SD}$  were both set to 0.5. This normalization process adjusts pixel intensity  $\mathbf{I}$  via the formula:

$$\mathbf{I}_{\text{norm}} = \frac{\mathbf{I} - \mu}{\sigma_{SD}} \quad (32)$$

where  $\mu$  and  $\sigma_{SD}$  are dataset-specific values.

Batch processing was performed with a batch size of  $B = 128$ , enabling efficient data handling and parallel processing. Once a batch reaches its end, the iterator is reset, ensuring a continuous data stream throughout training. This setup streamlined the flow of images into memory along with the generated feedback signals for each batch.

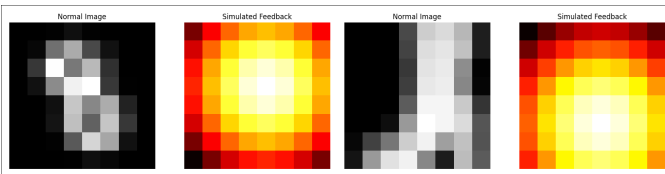


Fig. 1. A sample of preprocessed ( $8 \times 8$ ) pixel MNIST (left) and FashionMNIST (right) images and their corresponding feedback maps ( $\sigma = 5.0$ ).

##### B. Simulated Feedback Mechanism

To simulate supervisory guidance, we designed a feedback mechanism that highlights the most salient regions within each image via a Gaussian heatmap. The process begins with normalizing the input image  $I \in \mathbb{R}^{C \times H \times W}$  to a range of  $[0, 1]$ , defined by the transformation  $I_{\text{norm}} = \frac{I - \min(I)}{\max(I) - \min(I)}$ . This normalization ensures that all pixel values are scaled appropriately for subsequent computations. Next, the center of mass  $C$  of the image is identified, represented by the coordinates  $(x_c, y_c)$  corresponding to the pixel with the maximum intensity, calculated using  $C = \text{argmax}(I_{\text{norm}})$ . Utilizing these

coordinates, a Gaussian feedback mask  $M(x, y)$  is generated, which is centered around the identified pixel. The equation defines the Gaussian mask:

$$M(x, y) = \exp\left(-\frac{(x - x_c)^2 + (y - y_c)^2}{2\eta^2}\right) \quad (33)$$

where  $\eta = 5.0$  is a parameter that controls the spread of the Gaussian distribution, reflecting the degree of uncertainty in the feedback. This mask provides spatial feedback, where values decay radially from the center (see Figure 1). To ensure that the feedback mask is interpretable and usable within the model, it is normalized so that its maximum value equals 1:  $M_{\text{norm}} = \frac{M}{\max(M)}$ . The resulting normalized feedback mask effectively emphasizes regions within the image with higher intensity values, which aligns to guide the model’s attention toward salient features.

##### C. Resources Used

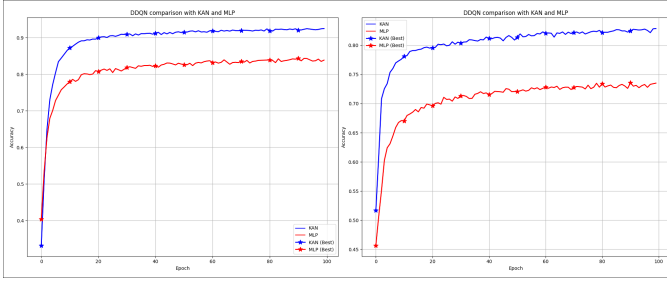
Our experiments were conducted via a setup powered by an Intel(R) Xeon(R) CPU with a clock speed of 2 GHz, 4 virtual CPU cores, and 16 GB of DDR4 RAM. The software environment included Python 3.10.12, with PyTorch for model development, PyKAN for KAN, Gymnasium for environment simulations, SciPy and NumPy for numerical computations, Matplotlib for data visualization, and SymPy for symbolic calculations.

##### D. Experimental Configurations

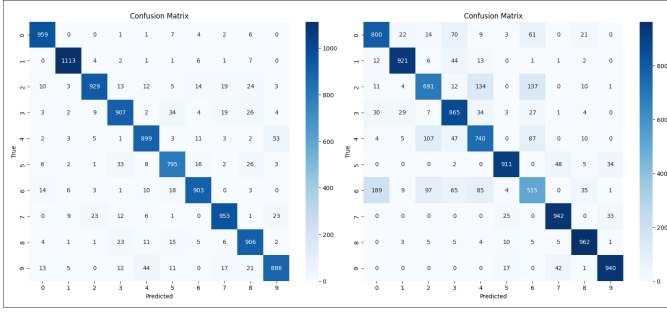
For the experiments conducted in this study, we employed two configurations for the MLP and KAN models, both set to a batch size of 128 and trained over 100 epochs. The configurations utilized a learning rate  $1 \times 10^{-3}$ , a weight decay  $1 \times 10^{-4}$ , and a discount factor ( $\gamma$ ) of 0.99. The MLP configuration featured a width of 32 and an output size of 10 classes, while the KAN configuration used a width of 8 and a grid size of 3. Both models share a common input size of 64 features, a buffer size 100,000, and a target update interval of 10. They incorporated warm-up episodes of 2 and utilized a beta distribution (see Table I) for their stochastic feature selection processes, with an initial  $\tau$  value set at 1.0. We strategically designed the architecture of our model by selecting the appropriate combination of convolutional layers and filters to ensure that the resulting selected feature map retains the same shape as the input and feedback size ( $64$  for  $8 \times 8$  images). This choice is crucial, as it directly allows the simulated feedback (similar to input size) to correspond to the feature map dimensions, facilitating effective integration during the feature selection process. In this case, for 1, 2, and 3 convolutional layers, we must select 2, 4, and 8 filter sizes to maintain the desired selected feature shape. The means and standard deviations for training and test accuracies are computed over a 10-epoch moving window to capture stability and uncertainty trends throughout training.

#### V. RESULTS

Our results reveal that KAN-DDQN outperforms MLP-DDQN in all cases on both MNIST and FashionMNIST

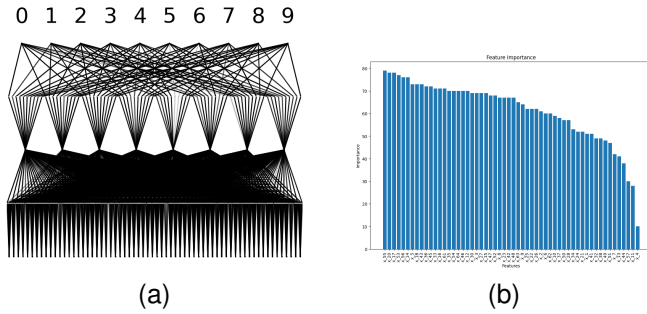


(a)



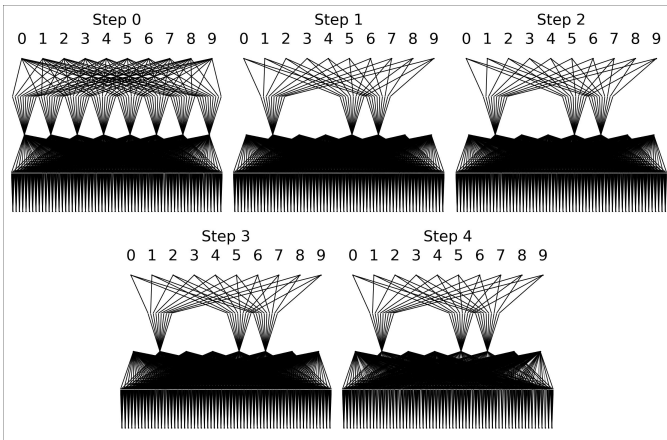
(b)

Fig. 2. Comparison of KAN and MLP-based DDQN on MNIST (left) and FashionMNIST (right) involving (a) training accuracy per epoch and (b) confusion matrix.



(a)

(b)



(c)

Fig. 3. (a) Pruned KAN architecture for MNIST, (b) feature importance plot obtained from the symbolic formula of the trained KAN agent, (c) training steps of our KAN agent for MNIST dataset.

datasets (see Fig. 2a and 2b) with 4 times fewer parameters and only  $8 \times 8$  sized images.

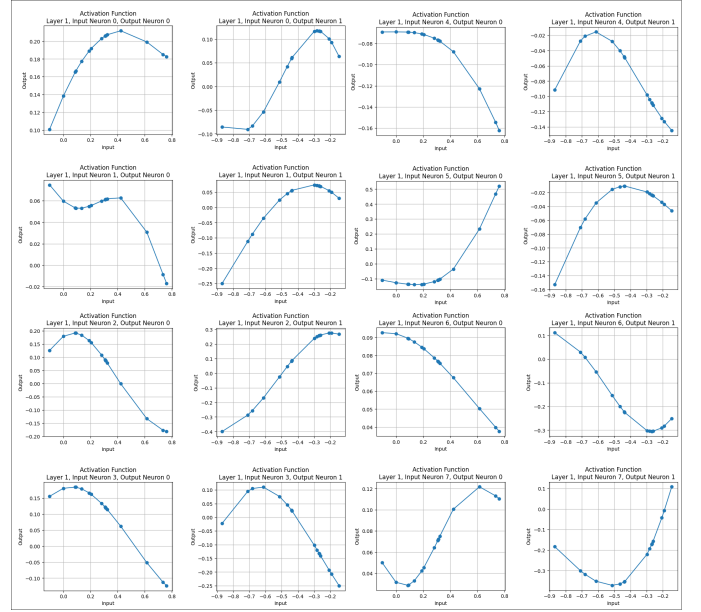


Fig. 4. Activation functions for middle neurons in KAN agent's hidden layer on MNIST dataset. Each subplot shows how a specific neuron transforms inputs via the spline activation, illustrating various activation behaviors across the layer.

TABLE I  
PERFORMANCE OF MLP-DDQN FOR DIFFERENT DISTRIBUTIONS ON MNIST AND FASHION MNIST DATASETS. **BOLD** INDICATES THE BEST PERFORMANCE.

Distribution	MNIST		FashionMNIST	
	Train Accuracy	Test Accuracy	Train Accuracy	Test Accuracy
Bernoulli	$0.57 \pm 0.03$	$0.58 \pm 0.00$	$0.55 \pm 0.02$	$0.54 \pm 0.00$
Gumbel Softmax	$0.15 \pm 0.01$	$0.18 \pm 0.00$	$0.10 \pm 0.02$	$0.24 \pm 0.00$
Gaussian	$0.22 \pm 0.01$	$0.21 \pm 0.00$	$0.22 \pm 0.01$	$0.21 \pm 0.01$
<b>Beta</b>	<b><math>0.79 \pm 0.02</math></b>	<b><math>0.78 \pm 0.00</math></b>	<b><math>0.68 \pm 0.01</math></b>	<b><math>0.66 \pm 0.00</math></b>
Dirichlet	$0.17 \pm 0.02$	$0.22 \pm 0.00$	$0.23 \pm 0.02$	$0.24 \pm 0.00$
Multinomial	$0.10 \pm 0.02$	$0.12 \pm 0.00$	$0.10 \pm 0.01$	$0.12 \pm 0.00$
Cauchy	$0.12 \pm 0.01$	$0.12 \pm 0.00$	$0.11 \pm 0.01$	$0.12 \pm 0.00$
Laplace	$0.16 \pm 0.02$	$0.18 \pm 0.00$	$0.21 \pm 0.01$	$0.19 \pm 0.00$
Uniform	$0.73 \pm 0.02$	$0.75 \pm 0.00$	$0.69 \pm 0.03$	$0.65 \pm 0.00$

#### A. Effect of Distribution Type in Feature Selection

Table I demonstrates significant variability in MLP-DDQN performance across different distributions for both MNIST and FashionMNIST datasets. We conducted this experiment to choose the best distribution that can mimic the human-like feature selection process. The beta distribution consistently yields the highest train and test accuracies on MNIST (79% and 78%, respectively), prompting us to conduct the remaining experiments with this distribution. Conversely, the Gumbel Softmax, Dirichlet, multinomial, Cauchy, and Laplace distributions perform poorly, with test accuracies as low as 12%. Notably, the uniform distribution also shows competitive results, particularly on the MNIST dataset, suggesting it can serve as a viable alternative for feature selection.

#### B. Effect of Feature Selection in Performance

1) *Performance With Feature Selection:* Table III illustrates the performance of the KAN-DDQN and standard MLP-DDQN using feature selection across MNIST and FashionMNIST datasets. In all cases, the hidden layer width was set to 32 neurons for the MLP and 8 for the KAN, reflecting



TABLE II  
PERFORMANCE METRICS WITHOUT FEATURE SELECTION ON MNIST AND FASHIONMNIST DATASETS USING KAN AND MLP MODELS.

Model	Dataset	No Feature Selection					Training Time (hh:mm:ss)
		maP	maR	maF1	Train Accuracy	Test Accuracy	
KAN	MNIST	0.57	0.57	0.56	0.56 ± 0.03	<b>0.58 ± 0.01</b>	5:10:50
MLP	MNIST	0.45	0.51	0.47	0.47 ± 0.02	0.52 ± 0.00	10:41
KAN	FashionMNIST	0.63	0.65	0.63	0.67 ± 0.02	<b>0.64 ± 0.00</b>	5:10:32
MLP	FashionMNIST	0.55	0.60	0.57	0.59 ± 0.02	0.59 ± 0.00	10:24

TABLE III  
PERFORMANCE COMPARISON OF KAN AND MLP MODELS ON MNIST AND FASHIONMNIST WITH FEATURE SELECTION

Model	Dataset	# Conv Layers	# Filters	# Width	Grid Size	With Feature Selection					Training Time (hh:mm:ss)
						maP	maR	maF1	Train Accuracy	Test Accuracy	
KAN	MNIST	1	2	8	3	0.92	0.92	0.92	0.93 ± 0.01	<b>0.93 ± 0.00</b>	4:35:26
MLP	MNIST	1	2	32	-	0.84	0.84	0.84	0.85 ± 0.02	0.84 ± 0.00	8:42
KAN	FashionMNIST	1	2	8	3	0.83	0.83	0.83	0.85 ± 0.01	<b>0.83 ± 0.00</b>	4:25:41
MLP	FashionMNIST	1	2	32	-	0.72	0.73	0.72	0.73 ± 0.01	0.74 ± 0.00	8:17
KAN	MNIST	2	4	8	3	0.73	0.73	0.73	0.75 ± 0.02	0.73 ± 0.00	5:50:29
MLP	MNIST	2	4	32	-	0.72	0.72	0.72	0.75 ± 0.02	0.72 ± 0.00	10:32
KAN	FashionMNIST	2	4	8	3	0.69	0.7	0.69	0.71 ± 0.01	0.70 ± 0.00	6:02:45
MLP	FashionMNIST	2	4	32	-	0.62	0.68	0.64	0.71 ± 0.02	0.68 ± 0.00	11:42

TABLE IV  
IMPACT OF KAN PARAMETER ADJUSTMENTS ON MNIST AND FASHIONMNIST PERFORMANCE

Model	Dataset	# Conv Layers	# Filters	# Width	Grid Size	With Feature Selection					Training Time (hh:mm:ss)
						maP	maR	maF1	Train Accuracy	Test Accuracy	
KAN	MNIST	2	4	8	2	0.72	0.72	0.72	0.72 ± 0.02	0.72 ± 0.00	6:05:24
KAN	MNIST	2	4	8	3	0.73	0.73	0.73	0.75 ± 0.02	0.73 ± 0.00	5:50:29
KAN	MNIST	2	4	<b>16</b>	<b>3</b>	0.75	0.74	0.74	0.74 ± 0.02	<b>0.75 ± 0.00</b>	10:21:59
KAN	FashionMNIST	2	4	8	2	0.70	0.71	0.70	0.72 ± 0.02	0.71 ± 0.00	5:11:51
KAN	FashionMNIST	2	4	8	3	0.69	0.70	0.69	0.71 ± 0.01	0.70 ± 0.00	6:02:45
KAN	FashionMNIST	2	4	<b>16</b>	<b>3</b>	0.71	0.72	0.71	0.73 ± 0.02	<b>0.72 ± 0.00</b>	11:41:30

the distinct architectures of each model. The KAN model consistently outperformed the MLP across all configurations, particularly on the MNIST dataset, achieving a test accuracy of 93% with a single convolutional layer, two filters, a width of 8, and a grid size of 3. For FashionMNIST, KAN similarly demonstrated superior test performance, reaching 83% accuracy under the same configuration, compared to MLP’s 74% accuracy. Across both datasets, KAN exhibited higher mean average precision (maP), recall (maR), and F1-score (maF1). For example, in the single-layer configuration on MNIST, KAN achieved scores of 0.92 for each metric, whereas MLP scored 0.84. The training time for the KAN model was generally longer because of its more intricate architecture, with the best-performing KAN model on MNIST requiring 4 hours and 35 minutes, compared with only 8 minutes for MLP (see Table III). Despite the increased computation, the accuracy gains suggest that KAN is efficient for applications where performance outweighs training time constraints. Notably, with the addition of a convolutional layer and increased filter size (e.g., 2 layers, 4 filters), KAN’s performance slightly declined, particularly on FashionMNIST, where test accuracy was 70%. This indicates a potential trade-off between model complexity and generalization, suggesting that simpler KAN configurations, particularly with a lower hidden layer width, may better retain discriminative power for smaller datasets.

2) *Performance Without Feature Selection:* Table II provides a comparative view of model performance without feature selection, highlighting the impact of excluding feature selection on both models’ performance. Without feature

selection, both KAN and MLP demonstrate considerably poor performance. Here, the KAN model achieves a notable decrease in test accuracy and maF1 compared with the MLP model. Specifically, on MNIST, KAN reaches a test accuracy of 58% with maF1 of 0.56, surpassing the MLP model’s 52% test accuracy and 0.47 maF1. On FashionMNIST, the KAN model continues to outperform, achieving a 64% test accuracy and 0.63 maF1, compared with MLP’s 59% accuracy and 0.57 maF1.

### C. Effect of KAN Parameters in Performance

Table IV shows how KAN performance varies with parameter adjustments, focusing on width (number of neurons in hidden layer) and grid size. Doubling the width of the feature maps from 8 to 16 yielded improvements in accuracy, especially on MNIST, where the test accuracy rose from 72% to 75%. However, this increase came at the expense of significantly longer training times, suggesting a trade-off between accuracy and computational efficiency. On FashionMNIST, similar parameter adjustments yielded more moderate gains. For example, increasing the grid size to 3 and width to 16 raised test accuracy slightly from 71% to 72%. Moreover, altering the grid size from 2 to 3 produces varied outcomes: it preserves similar test accuracy in MNIST (0.72 to 0.73) but slightly decreases performance in FashionMNIST (0.71 to 0.70). This variation may stem from applying the B-spline in higher dimensions, warranting further exploration. This pattern suggests that KAN’s parameter sensitivity is dataset-dependent, with MNIST benefiting more from only width

increases. Training time increased substantially with larger configurations. On MNIST, the KAN model with a grid size of 3 and width of 16 took over 10 hours, while the smaller grid size of 2 and width of 8 configurations was completed in 6 hours. Thus, reducing width and grid size may be advantageous for time-sensitive applications, especially where marginal accuracy improvements are not critical. So, larger hidden layer widths improve KAN’s accuracy but at the cost of increased training time. Balancing grid size and width for applications prioritizing efficiency may offer an optimal trade-off without sacrificing significant accuracy.

#### D. Interpretability of KAN-DDQN

In our KAN-DDQN architecture, several interpretability features improve the understanding of the model’s decision-making process, particularly after training on datasets.

1) *Pruning*: After training, we implement a pruning mechanism to streamline the KAN architecture by eliminating less important neurons (see Fig. 3a). The significance of a neuron is determined by its incoming and outgoing scores, defined as:

$$I_{l,i} = \max_k(|\phi_{l-1,i,k}|_1), \quad O_{l,i} = \max_j(|\phi_{l+1,j,i}|_1) \quad (34)$$

A neuron is considered important if both its incoming score  $I_{l,i}$  and outgoing score  $O_{l,i}$  exceed a threshold  $\theta = 10^{-2}$ . Unimportant neurons not meeting this criterion are pruned from the network, resulting in a more efficient model.

2) *Visualization*: To understand the importance of features, we utilize the plotting functionality of the KAN model. Fig. 3a visualizes the activation functions of the neurons, and Fig. 3c shows the training steps of the KAN agent where the bottom layer indicates 64 input variables, followed by 8 hidden neurons and then 10 outputs. The transparency of each activation function  $\phi_{l,i,j}$  is set proportionally to  $\tanh(\beta A_{l,i,j})$ , where  $\beta = 30$ . Smaller  $\beta$  allows us to focus on more significant activations.

3) *Symbolification*: Our approach identifies symbolic forms within the KAN architecture to enhance interpretability. We sample network preactivations  $x$  and post-activations  $y$ , fitting an affine transformation  $y \approx cf(ax + b) + d$ , where  $a, b$  adjust inputs, and  $c, d$  scale and shift outputs. This fitting involves grid search on  $a, b$  and linear regression for  $c, d$ . Using a library of symbolic functions ( $x, x^2, x^3, \exp(x), \log(x), \sqrt{x}, \sin(x), |x|$ ), auto-symbolic regression replaces learned activations with interpretable formulas. The policy in KAN-DDQN is represented as  $a_i = f_i(x)$  for each output  $i$ , with the overall action  $a = \underset{i}{\operatorname{argmax}} a_i$ . Fig. 3b displays the importance of features extracted from a symbolic formula, showing their frequency of occurrence and corresponding contributions to the model’s predictions. Fig. 4 illustrates the activation function of a middle neuron in the KAN’s 8-neuron hidden layer for two input neurons, with the x-axis showing input values and the y-axis indicating the activation output after the spline function.

## VI. CONCLUSION AND FUTURE WORK

This study introduced a HITL feature selection framework using a DDQN architecture with KAN, achieving inter-

pretable, per-example feature selection and improved performance across multiple metrics. Through simulated feedback and stochastic feature sampling from diverse distributions, the HITL-KAN-DDQN model dynamically selects feature subsets for each observation, focusing on the most relevant features and improving interpretability. Operating on low-resolution  $8 \times 8$  pixel images, our model consistently outperforms MLP-based DDQN models, achieving higher accuracy while using fewer neurons—specifically, an 8-neuron single hidden layer compared to the 32-neuron layer required by the MLP-DDQN. This compact design provided computational efficiency without compromising predictive power, confirming the effectiveness of the HITL-KAN-DDQN model for feature selection.

Future work could improve simulated feedback to align better with expert annotations and apply this HITL approach to various feature selection tasks and high-dimensional domains. Exploring RL further may involve querying feedback based on model uncertainty or data point importance, moving toward active learning. Other RL policies to explore include DQN, REINFORCE, proximal policy optimization (PPO), advantage actor-critic (A2C), and soft actor-critic (SAC).

## REFERENCES

- [1] I. Guyon and A. Elisseeff, “An introduction to variable and feature selection,” *J. Mach. Learn. Res.*, vol. 3, no. null, pp. 1157–1182, Mar. 2003.
- [2] G. Chandrashekar and F. Sahin, “A survey on feature selection methods,” *Computers & Electrical Engineering*, vol. 40, no. 1, pp. 16–28, Jan. 2014. [Online]. Available: <https://doi.org/10.1016/j.compeleceng.2013.11.024>
- [3] A. H. C. Correia and F. Lecue, “Human-in-the-Loop Feature Selection,” *Proceedings of the AAAI Conference on Artificial Intelligence*, vol. 33, no. 01, pp. 2438–2445, Jul. 2019, number: 01. [Online]. Available: <https://doi.org/10.1609/aaai.v33i01.33012438>
- [4] S. Kumar, S. Datta, V. Singh, D. Datta, S. Kumar Singh, and R. Sharma, “Applications, Challenges, and Future Directions of Human-in-the-Loop Learning,” *IEEE Access*, vol. 12, pp. 75 735–75 760, 2024. [Online]. Available: <https://doi.org/10.1109/ACCESS.2024.3401547>
- [5] X. Wu, L. Xiao, Y. Sun, J. Zhang, T. Ma, and L. He, “A survey of human-in-the-loop for machine learning,” *Future Generation Computer Systems*, vol. 135, pp. 364–381, Oct. 2022. [Online]. Available: <https://doi.org/10.1016/j.future.2022.05.014>
- [6] H. v. Hasselt, A. Guez, and D. Silver, “Deep reinforcement learning with double Q-Learning,” in *Proceedings of the Thirtieth AAAI Conference on Artificial Intelligence*, ser. AAAI’16. Phoenix, Arizona: AAAI Press, Feb. 2016, pp. 2094–2100.
- [7] H. Raghavan, O. Madani, and R. Jones, “Active Learning with Feedback on Features and Instances,” *J. Mach. Learn. Res.*, vol. 7, pp. 1655–1686, Dec. 2006.
- [8] A. Verma, V. Murali, R. Singh, P. Kohli, and S. Chaudhuri, “Programmatically Interpretable Reinforcement Learning,” in *Proceedings of the 35th International Conference on Machine Learning*. PMLR, Jul. 2018, pp. 5045–5054, iSSN: 2640-3498. [Online]. Available: <https://proceedings.mlr.press/v80/verma18a.html>
- [9] A. Cano, A. R. Masegosa, and S. Moral, “A Method for Integrating Expert Knowledge When Learning Bayesian Networks From Data,” *IEEE Transactions on Systems, Man, and Cybernetics, Part B (Cybernetics)*, vol. 41, no. 5, pp. 1382–1394, Oct. 2011. [Online]. Available: <https://doi.org/10.1109/TSMCB.2011.2148197>
- [10] H.-N. Wu, W.-H. Li, and M. Wang, “A Finite-Horizon Inverse Linear Quadratic Optimal Control Method for Human-in-the-Loop Behavior Learning,” *IEEE Transactions on Systems, Man, and Cybernetics: Systems*, vol. 54, no. 6, pp. 3461–3470, Jun. 2024. [Online]. Available: <https://doi.org/10.1109/TSMC.2024.3357973>
- [11] Z. Liu, Y. Wang, S. Vaidya, F. Ruehle, J. Halverson, M. Soljačić, T. Y. Hou, and M. Tegmark, “KAN: Kolmogorov-Arnold Networks,” Jun. 2024, arXiv:2404.19756 [cond-mat, stat]. [Online]. Available: <https://doi.org/10.48550/arXiv.2404.19756>